Matrix Isolation Infrared Spectroscopic and Theoretical Study of the Hydrolysis of Boron Dioxide in Solid Argon

Yu Gong and Mingfei Zhou*

Department of Chemistry, Shanghai Key Laboratory of Molecular Catalysts and Innovative Materials, Advanced Materials Laboratory, Fudan University, Shanghai 200433, P. R. China

Received: February 18, 2008; Revised Manuscript Received: April 9, 2008

The reaction of boron dioxide with water molecule has been studied using matrix isolation infrared spectroscopy. The boron dioxide molecules produced by codeposition of laser-evaporated boron atoms with dioxygen react spontaneously with water molecules to form $OB(OH)_2$, which is characterized to have a doublet ground-state with two OH groups in the cis−trans form. Isotopic substitution results indicate that the hydrolysis process proceeds via a concerted two hydrogen atom transfer mechanism. The *cis*−*trans*-$OB(OH)_2$ molecule is photosensitive; it decomposes to the OH·OB(OH) complex upon broadband UV−visible irradiation. The OH·OB(OH) complex is determined to have a $^2A''$ ground-state with a bent C_s symmetry, in which the terminal oxygen atom of the OB(OH) fragment is hydrogen bonded with the hydroxyl radical. The OH·OB(OH) complex recombines to the *cis*−*trans*-$OB(OH)_2$ molecule upon sample annealing.

Introduction

Solid boron and boron-containing materials are regarded as effective fuels with high energy density in the field of aerospace. Upon boron oxidation during the combustion process, the existence of water leads to the partial formation of boron oxyhydrides instead of pure boron oxide, which reduces the energy released.[1] Investigations on the hydrolysis of boron oxide at the molecular level serve as a simple model for understanding the related mechanisms of bulk materials. The hydrolysis products of boron oxide are mainly orthoboric acid $B(OH)_3$ and metaboric acid OB(OH), which have been the subject of several experimental studies both in the gas phase and in solid matrix. Attinà et al. investigated the positive and negative ion chemistry of orthoboric, metaboric, and polyboric acids using a combination of chemical ionization and ion cyclotron resonance mass spectrometry. A series of new charged species were characterized.[2] Ortho- and metaboric acids, $B(OH)_3$ and OB(OH), were identified as the major vapor species in the $B_2O_3-H_2O$ or bulk $B(OH)_3$ systems by vibrational spectroscopic and mass spectrometric studies.[3–6] The infrared spectra of isolated molecular $B(OH)_3$ and OB(OH) were also reported in solid noble gas matrixes.[7,8] The orthoboric acid molecule isolated in matrixes was characterized to have a C_{3h} symmetry. The OB(OH) molecule was the major thermal decomposition product from laser evaporation of bulk $B(OH)_3$ target, which was predicted to possess a bent C_s geometry. The structures and vibrational frequencies of molecular $B(OH)_3$ and OB(OH) and their clusters have also been explored by quantum chemical calculations.[9–16]

To our knowledge, there is no experimental report on the reactions between water and molecular boron oxides except a guided ion beam mass spectrometric study on the reactions of $B_nO_m^+$ and $B_nO_mH^+$ cluster cations with D_2O.[17] Herein, we report a combined matrix isolation infrared spectroscopic and theoretical study on the reactions of molecular boron dioxide with water in solid argon. The hydrolysis product of boron dioxide, $OB(OH)_2$, was trapped and identified, which further decomposes to the hydrogen-bonded OH·OB(OH) complex upon broad-band UV−visible irradiation.

Experimental and Computational Methods

The experimental setup for pulsed laser evaporation and matrix isolation infrared spectroscopic investigation has been described in detail previously.[18] Briefly, the 1064 nm fundamental of a Nd:YAG laser (Continuum, Minilite II, 10 Hz repetition rate and 6 ns pulse width) was focused onto a rotating boron target through a hole in a CsI window cooled normally to 6 K by means of a closed-cycle helium refrigerator (ARS, 202N). The laser-evaporated boron atoms were codeposited with O_2/H_2O/Ar mixtures onto the CsI window. In general, matrix samples were deposited for 1 h at a rate of approximately 4 mmol/h. The O_2/H_2O/Ar mixtures were prepared in a stainless steel vacuum line using a standard manometric technique. Natural abundance boron (^{10}B, 19.8%; ^{11}B, 80.2%) and isotopic ^{10}B-enriched targets were used in the experiments. H_2O and $H_2{}^{18}O$ (Cambridge Isotopic Laboratories) were subjected to several freeze−pump−thaw cycles to minimize possible atmospheric contamination. Isotopic $^{18}O_2$ (ISOTEC, 99%) was used without further purification. The infrared absorption spectra of the resulting samples were recorded on a Bruker IFS 66V spectrometer at 0.5 cm^{-1} resolution between 4000 and 450 cm^{-1} using a liquid nitrogen cooled HgCdTe (MCT) detector. Samples were annealed to different temperatures and cooled back to 6 K for spectral acquisition. Selected samples were subjected to broad-band irradiation ($250 < \lambda < 580$ nm) using a high-pressure mercury arc lamp.

Quantum chemical calculations were performed using the Gaussian 03 program.[19] The three-parameter hybrid functional according to Becke with additional correlation corrections due to Lee, Yang, and Parr (B3LYP) was utilized.[20,21] The 6-311++G(d,p) basis set was used for all the calculations.[22] The geometries were fully optimized; the harmonic vibrational frequencies were calculated, and zero-point vibrational energies (ZPVE) were derived. The single point energies of all the structures optimized at the B3LYP level of theory were calculated using the CCSD(T) method with the same basis set.

* Corresponding author. E-mail: mfzhou@fudan.edu.cn.

10.1021/jp8014172 CCC: $40.75
Published on Web 05/30/2008

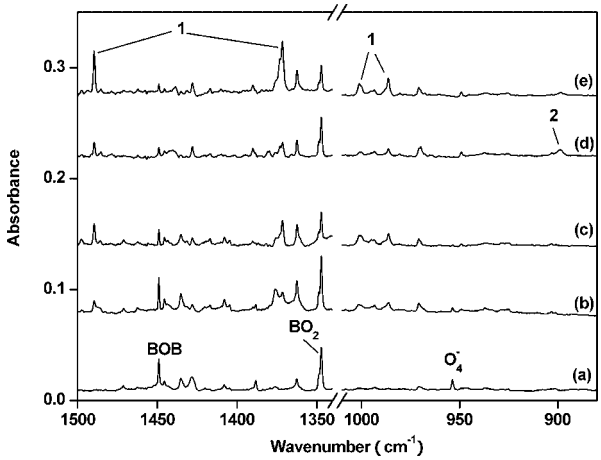

Figure 1. Infrared spectra in the 1500−1340 and 1010−880 cm^{-1} regions from codeposition of laser-evaporated ^{10}B with 0.05% H_2O + 0.5% O_2 in argon: (a) 1 h of sample deposition at 6 K, (b) after 25 K annealing, (c) after 35 K annealing, (d) after 15 min of 250 < λ < 580 nm irradiation, and (e) after 35 K annealing.

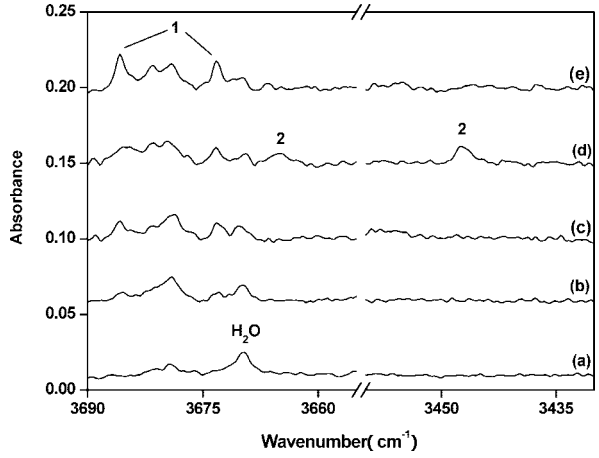

Figure 2. Infrared spectra in the 3690−3655 and 3460−3430 cm^{-1} regions from codeposition of laser-evaporated ^{10}B with 0.05% H_2O + 0.5% O_2 in argon: (a) 1 h of sample deposition at 6 K, (b) after 25 K annealing, (c) after 35 K annealing, (d) after 15 min of 250 < λ < 580 nm irradiation, and (e) after 35 K annealing.

Results and Discussions

Infrared Spectra. The boron dioxide molecules were prepared by codeposition of laser-evaporated boron atoms with dioxygen in excess argon. In order to minimize the formation of multinuclear species, the experiments were performed with relatively low laser energy (approximately 10 mJ/pulse) using different ratios of O_2/H_2O mixtures in excess argon. The spectra in selected regions via codeposition of laser-evaporated boron atoms from a ^{10}B-enriched target using a 0.5% O_2 + 0.05% H_2O/Ar sample are shown in Figures 1 and 2, respectively, with the product absorptions listed in Table 1. After 1 h of sample deposition at 6 K, the spectrum (Figure 1, trace a) is dominated by the absorptions of $^{10}BO_2$ and $^{10}BO^{10}B$, which were previously identified in the reactions of boron atoms and O_2 in solid argon.[23] Weak absorptions due to O_4^- (953.6 cm^{-1}),[24] ^{10}BO (1907.7 cm^{-1}),[23] and $H^{10}BO$ (1861.0 cm^{-1})[25] were also observed. When the as-deposited sample was annealed at high temperatures (Figures 1 and 2, traces b and c), a series of new absorptions at 3686.0, 3673.5, 1489.7, 1371.5, 1001.3, 986.3, and 673.5 cm^{-1} was produced that was absent in the experiments using O_2 and H_2O separately.[23,25] These absorptions retain constant relative IR intensities throughout all the experiments, indicating that they

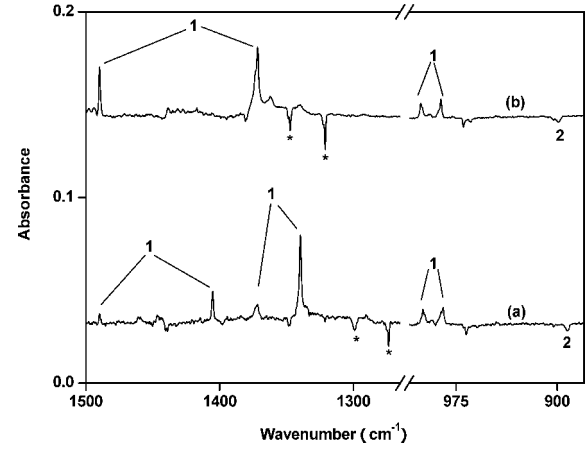

Figure 3. Difference spectra in the 1500−1265 and 1010−880 cm^{-1} regions (spectrum taken after 35 K annealing minus spectrum taken after 15 min of 250 < λ < 580 nm irradiation) with 0.05% H_2O + 0.5% O_2 in argon: (a) natural abundance boron and (b) ^{10}B-enriched boron. The asterisks denote the absorptions of $^{11}BO_2$ and $^{10}BO_2$.

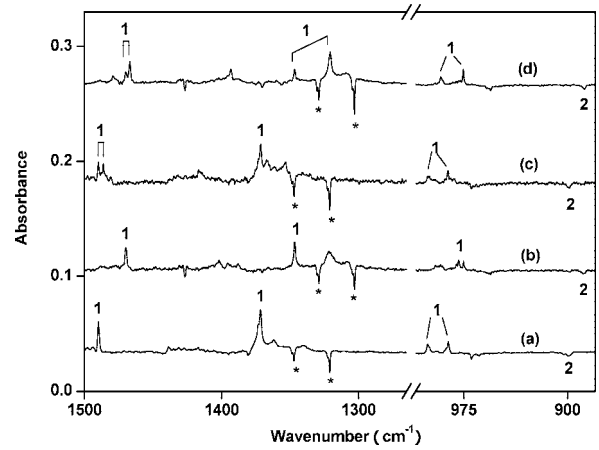

Figure 4. Difference spectra in the 1500−1265 and 1010−880 cm^{-1} regions (spectrum taken after 35 K annealing minus spectrum taken after 15 min of 250 < λ < 580 nm irradiation) with a ^{10}B-enriched boron target: (a) 0.05% H_2O + 0.5% O_2, (b) 0.05% H_2O + 0.5% $^{18}O_2$, (c) 0.05% $H_2{}^{18}O$ + 0.5% O_2, and (d) 0.05% $H_2{}^{18}O$ + 0.5% $^{18}O_2$. The asterisks denote the absorptions of $^{10}B^{16}O_2$ and $^{10}B^{18}O_2$.

are due to different vibrational modes of the same species, and they are assigned to product **1**. The IR intensities due to product **1** decreased when the sample was subjected to broad-band irradiation (250 < λ <580 nm), during which another group of absorptions at 3665.3, 3447.5, and 898.8 cm^{-1} was produced (Figures 1 and 2, trace d). The absorptions at 3665.3, 3447.5, and 898.8 cm^{-1} were attributed to species **2**. When the irradiated sample was further annealed to 35 K (Figures 1 and 2, trace e), the absorptions due to product **2** disappeared, while the absorptions of product **1** increased.

Experiments were performed with a natural abundance boron target; a difference spectrum in selected regions from the spectrum taken after 35 K annealing minus the spectrum taken after 15 min of 250 < λ < 580 nm irradiation is illustrated in Figure 3. Some modes of product**1** and **2** split into doublet with natural abundance boron. The ^{11}B counterparts are also listed in Table 1.

Experiments were also repeated using the isotopic-labeled $^{18}O_2$ + $H_2{}^{16}O$, $^{16}O_2$ + $H_2{}^{18}O$, and $^{18}O_2$ + $H_2{}^{18}O$ mixtures with the ^{10}B-enriched target. The spectra in selected regions with different isotopic samples are shown in Figures 4−6, respectively, with the isotopic counterparts summarized in Table 1.

TABLE 1: Infrared Absorptions (cm^{-1}) of $OB(OH)_2$ and $OH·OB(OH)$ in Solid Argon

^nB[a]	^{10}B					
$^{16}O_2 + H_2{}^{16}O$	$^{16}O_2 + H_2{}^{16}O$	$^{18}O_2 + H_2{}^{16}O$	$^{16}O_2 + H_2{}^{18}O$	$^{18}O_2 + H_2{}^{18}O$	assignment	
3686.0	3686.0	3674.7	3686.0	3674.7	OH str	$OB(OH)_2$
3673.5	3673.5	3662.2	3673.5	3662.2	OH str	
1405.2, 1489.7	1489.7	1469.8	1489.7[b]	1469.8[b]	B-OH str	
			1486.2	1466.8		
1339.7, 1371.5	1371.5	1346.8	1371.5	1346.8[b]	B-OH str	
				1320.9,		
999.6,	1001.3		1001.3	991.8	BOH bend	
984.8, 986.3	986.3	975.5	986.3	975.5	BOH bend	
648.0, 673.5	673.5		673.5,[b] 671.3		BO_3 def	
3665.3	3665.3	3653.7	3665.3	3653.7	OH str	OH·OB(OH)
3447.5	3447.5	3436.4	3447.5	3436.4	OH str	
2037.0		2084.0		2084.0	B═O str	
892.5	898.8	888.4	898.8	887.8	BOH bend	

[a] ^nB denotes natural abundance boron (^{10}B, 19.8%;^{11}B, 80.2%). [b] Absorptions due to the presence of $H_2{}^{16}O$ in the mixed samples.

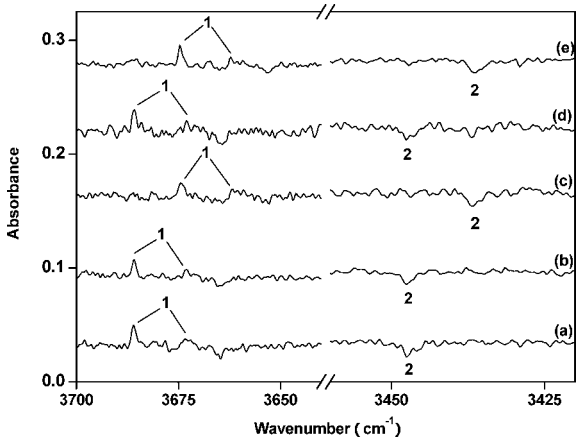

Figure 5. Difference spectra in the 3700−3640 and 3460−3420 cm^{-1} regions (spectrum taken after 35 K annealing minus spectrum taken after 15 min of 250 < λ < 580 nm irradiation) with different isotopic samples: (a) natural abundance boron, 0.05% H_2O + 0.5% O_2, (b) ^{10}B-enriched boron, 0.05% H_2O + 0.5% O_2, (c) ^{10}B-enriched boron, 0.05% H_2O + 0.5% $^{18}O_2$, (d) ^{10}B-enriched boron, 0.05% $H_2{}^{18}O$ + 0.5% O_2, and (e) ^{10}B-enriched boron, 0.05% $H_2{}^{18}O$ + 0.5% $^{18}O_2$.

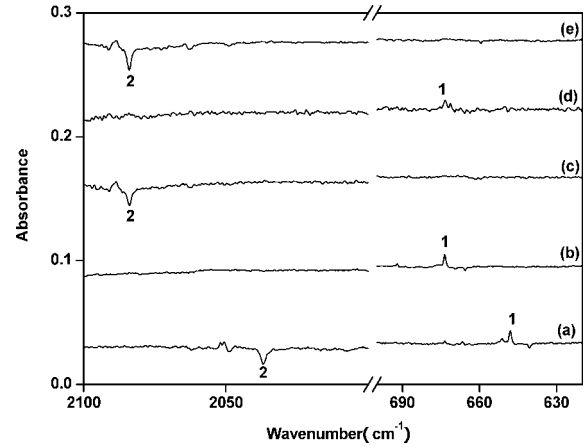

Figure 6. Difference spectra in the 2100−2000 and 700−620 cm^{-1} regions (spectrum taken after 35 K annealing minus spectrum taken after 15 min of 250 < λ < 580 nm irradiation) with different isotopic samples: (a) natural abundance boron, 0.05% H_2O + 0.5% O_2, (b) ^{10}B-enriched boron, 0.05% H_2O + 0.5% O_2, (c) ^{10}B-enriched boron, 0.05% H_2O + 0.5% $^{18}O_2$, (d) ^{10}B-enriched boron, 0.05% $H_2{}^{18}O$ + 0.5% O_2, and (e) ^{10}B-enriched boron, 0.05% $H_2{}^{18}O$ + 0.5% $^{18}O_2$.

$OB(OH)_2$. The absorptions at 3686.0, 3673.5, 1489.7, 1371.5, 1001.3, 986.3, and 673.5 cm^{-1} (product **1**) with ^{10}B-enriched target appeared on sample annealing at the expense of BO_2. These absorptions were absent in the experiments using O_2 and H_2O separately and are assigned to different vibrational modes of the $O^{10}B(OH)_2$ molecule. When the natural abundance boron target was used, a series of doublet patterns at 1489.7/1405.2, 1371.5/1339.7, 986.3/984.8, and 673.5/648.0 cm^{-1} were produced with relative intensities of approximately of 1:4 (Figure 3), which clearly demonstrates the involvement of only one boron atom in this molecule. The 3686.0 and 3673.5 cm^{-1} absorptions exhibit no $^{10}B/^{11}B$ shift, but they shifted to 3674.7 and 3662.2 cm^{-1} when the mixed $^{18}O_2 + H_2{}^{18}O$ sample was used. The $^{16}O/^{18}O$ isotopic frequency ratio was determined to be 1.0031 for both modes. Both the band positions and isotopic frequency ratios indicate that these two absorptions are due to O−H stretching vibrations. The 1489.7 and 1371.5 cm^{-1} absorptions are predominantly B-OH stretching vibrations, while the 1001.3 and 986.3 cm^{-1} absorptions are due to the BOH bending vibrations based on their isotopic shifts (Table 1). The vibrational frequencies of these modes are very close to those of $B(OH)_3$ in solid argon.[7,8]

To confirm the assignment and to get further insight into the structure and bonding of the $OB(OH)_2$ molecule, quantum chemical calculations were performed on this species. As shown in Figure 7, three conformers with different orientations of the hydroxyl groups were found to be stable. At the B3LYP/6−311++G(d,p) level of theory, two of them in which the OH groups are in the form of cis−cis with a C_{2v} symmetry and cis−trans with a planar C_s structure were predicted to be nearly degenerate, while the trans−trans isomer with a nonplanar C_2 symmetry lies about 5 kcal/mol higher in energy than the other two isomers. In order to determine the relative stability of the three isomers, more reliable single point energy calculations at the CCSD(T)//B3LYP/6−311++G(d,p) level of theory were carried out. The calculation results show that the cis−trans form in a $^2A'$ ground state is 0.6 kcal/mol lower in energy than the cis−cis isomer. The calculated vibrational frequencies of the observed modes are in quite good agreement with the experimental values (Tables 2 and 3). The calculated isotopic frequency ratios are also in good agreement with the observed values except for the two B-OH stretching modes (Table 3). The predicted $^{10}B/^{11}B$ ratio for the upper mode is lower, whereas the predicted $^{10}B/^{11}B$ ratio for the lower mode is higher than the experimental values. Similar behavior has been reported for the B-OH stretching modes of the $B(OH)_3$ molecule.[8] As has been discussed, Fermi resonance is responsible for the anomalous isotopic ratios of $B(OH)_3$.

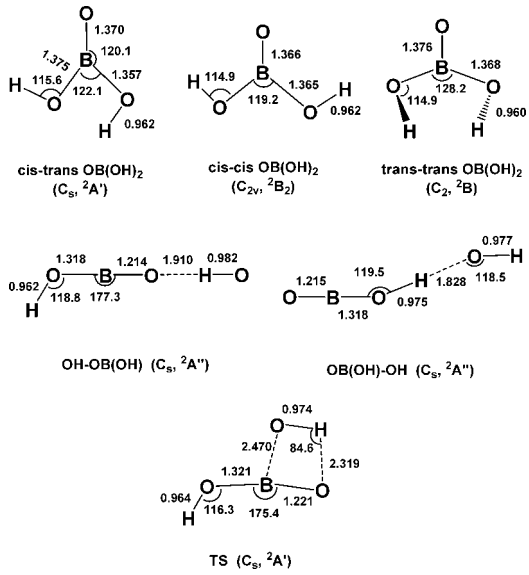

Figure 7. Optimized structures (DFT/B3LYP) of the species mentioned in the text (bond lengths in angstrom and bond angles in degrees).

As shown in Figure 7, the terminal B−O distance in the cis−trans form of $OB(OH)_2$ was predicted to be 1.370 Å, which is about the same as that of the B−O single bond (1.367 Å) in crystalline orthoboric acid.[26] Population analysis shows that the unpaired electron is mainly located on the terminal oxygen atom (0.95e). Therefore, doublet $OB(OH)_2$ is a univalent radical $•OB(OH)_2$.

Although the structure of neutral $OB(OH)_2$ molecule has not yet been determined, the existence of the corresponding $[OB(OH)_2]^-$ anion has been confirmed and characterized by mass spectrum[2b] and single crystal X-ray diffraction.[27] The structure of the borate anion in solid state revealed a similar structure as the $OB(OH)_2$ molecule reported here, in which the two hydroxyl groups were also in the cis−trans form. But the BO bond length in the $[OB(OH)_2]^-$ anion is shorter than that in the neutral species due to the addition of an extra electron to the SOMO of $OB(OH)_2$ molecule, which is mainly the in-plane π bonding orbital of boronyl in character.

OH·OB(OH) Complex. The absorptions at 3665.3, 3447.5, and 898.8 cm^{-1} (product **2**) using ^{10}B-enriched target were produced upon broadband irradiation at the expense of the $OB(OH)_2$ absorptions, which implies that species **2** is most likely due to a photolysis product of $OB(OH)_2$. Extra absorptions were observed at 2037.0 and 892.5 cm^{-1} when a natural abundance boron target was used. The 3665.3 cm^{-1} absorption is due to an O−H stretching vibration based on the band position and isotopic frequency ratio. The much weaker absorptions at 898.8/892.5 cm^{-1} are the corresponding in-plane BOH bending mode. The absorption at 2037.0 cm^{-1} was observed only in the experiment with natural abundance boron target. Although its ^{10}B counterpart was absent in the experiment with H_2O/O_2, this mode was observed at 2084.0 cm^{-1} with $H_2O/^{18}O_2$. The band position suggests a terminal *B*═O stretching vibration. These observations indicate that product **2** involves a OB(OH) fragment. The band positions are slightly shifted from those of the isolated metaboric acid molecule in solid argon,[8] which suggests that product **2** is a OB(OH) complex weakly perturbed by another fragment. The 3447.5 cm^{-1} absorption exhibits no shift upon ^{11}B substitution, but it shifted to 3436.4 cm^{-1} with $^{18}O_2/H_2O$. The $^{16}O/^{18}O$ ratio of 1.0032 indicates a typical OH stretching vibration. The band position is 100.7 cm^{-1} red-shifted from the free OH radical in solid argon (3548.2 cm^{-1})[28] and is very close to the O−H stretching vibration of the $H_2O·HO$ complex (3452.2 cm^{-1}).[29] Accordingly, absorptions **2** are assigned to the OH·OB(OH) complex.

Theoretical calculations were performed on the OH·OB(OH) complex. Two geometries were optimized at the B3LYP level: a OH·OB(OH) structure with the terminal oxygen atom of the OB(OH) fragment to be hydrogen bonded with the hydroxyl radical and a OB(OH)·OH complex with the oxygen atom of the hydroxyl radical being hydrogen bonded with the OB(OH) fragment. For the OH·OB(OH) complex, two states corresponding to the unpaired electron residing in the in-plane ($^2A'$) and out-of-plane ($^2A''$) 2p orbitals of oxygen are almost degenerate (Table 2), with the $^2A''$ state slightly lower in energy. Both states show about the same geometric structure and vibrational frequencies. The OH·OB(OH) complex has a H−OB(HO) distance of 1.910 Å, slightly longer than that of the OB(OH)·OH complex (1.828 Å). These two hydrogen-bonded complexes are very close in energy, with the OB(OH)·OH complex being only 0.7 kcal/mol lower in energy than the OH·OB(OH) complex. On the basis of the calculated frequencies, the experimentally observed frequencies should be assigned to the OH·OB(OH) complex instead of the OB(OH)·OH complex. As listed in Table 2, both complexes were predicted to have strong O−H stretching vibration of the hydroxyl fragment around 3600 cm^{-1}, about 100 cm^{-1} red-shifted from that of the OH radical calculated at the same level of theory, which fits the experimental value of 100.7 cm^{-1}. The O−H stretching, *B*═O stretching, and BOH bending modes of the HOBO fragment in $OH·O^{11}B(OH)$ were computed at 3875.9, 2083.4, and 916.2 cm^{-1}, which are in good agreement with the experimental values. These three modes of the OB(OH)·OH complex were calculated at 3699.9, 2073.5, and 1032.7 cm^{-1}. The O−H stretching frequency is too low whereas the BOH bending mode is too high to fit the experimental values.

The bonding of OH·OB(OH) complex is quite similar to that of the recently reported $H_2O·HO$ complex, which was determined to have a nonplanar C_s structure with the oxygen atom of H_2O hydrogen bonded with the hydroxyl radical.[29–31] The hydrogen bond distance in the $H_2O·HO$ complex was predicted to be around 1.95 Å using both ab initio and DFT methods, which is very similar to that of the OH·OB(OH) complex characterized here. The hydrogen-bonded $H_2O·HO$ complex was predicted to have a binding energy of approximately 5 kcal/mol, about the same as that of the OH·OB(OH) complex (5.8 kcal/mol) calculated at the CCSD(T)//DFT/B3LYP level of theory. Accordingly, these two hydrogen-bonded complexes showed very similar O−H stretching vibrational frequencies in solid argon (3447.5 versus 3452.2 cm^{-1}). The OH·OB(OH) complex is sufficiently strongly bound that BSSE corrections can be neglected (less than 0.5 kcal/mol).

Reaction Mechanism. The experimental observations lead us to propose the following reactions (Scheme 1):

SCHEME 1

$$B + O_2 \xrightarrow{\text{annealing}} BO_2 \xrightarrow{H_2O} OB(OH)_2 \underset{\text{annealing}}{\overset{250<\lambda<580\text{nm}}{\rightleftharpoons}} OH\text{-}OB(OH)$$

Laser evaporated boron atoms react with O_2 molecules to form the inserted linear boron dioxide molecules, which has been discussed previously.[23] Subsequent sample annealing in the presence of water molecules allows the reactants to diffuse and react. The *cis*−*trans*-$OB(OH)_2$ molecules were formed via the reaction of BO_2 and H_2O. This process was predicted to be exothermic by about 47.1 kcal/mol at the CCSD(T)//B3LYP level of theory.

TABLE 2: DFT/B3LYP Calculated Total Energies[a] and Frequencies (cm^{-1}) and Intensities (km/mol) of the Species Mentioned in the Text

molecule	energy	frequency (intensity)
cis−*trans*-$O^{11}B(OH)_2$ (C_s, $^2A'$)	−251.854 079 (−251.309 41)	3864.7 (96), 3863.0 (96), 1459.9 (311), 1323.6(329), 994.7 (85), 978.8 (149), 872.6(4), 642.1 (62), 439.4 (1), 412.0 (24), 361.4 (16), 334.2 (278)
cis−*cis*-$O^{11}B(OH)_2$ (C_{2v}, $^2B_2$)	−251.854 591 (−251.308 424)	3877.8 (7), 3875.8 (208), 1368.4 (274), 1351.8(202), 992.1 (51), 983.5 (232), 875.9(1), 639.8 (65), 446.4 (271), 423.6 (2), 325.4 (27), 315.5 (0)
trans−*trans*-$O^{11}B(OH)_2$ (C_2, ^2B)	−251.846 637 (−251.302 621)	3887.3 (139), 3882.1 (31), 1419.3 (211), 1387.7(492), 967.1 (71), 929.3 (219), 868.9(0), 636.5 (64), 428.0 (16), 412.1 (71), 329.6 (168), 201.5 (15)
OH·$O^{11}B(OH)$ (C_s, $^2A''$)	−251.789 805 (−251.241 346)	3875.9 (212), 3600.5 (391), 2083.4 (553), 1044.3 (2), 916.2 (195), 517.9 (83), 493.8(168),458.4 (27), 425.8 (140), 157.1 (4), 28.1 (1), 14.3 (3)
OH·$O^{11}B(OH)$ (C_s, $^2A'$)	−251.789 770 (−251.241 305)	3876.0 (213), 3600.5 (392), 2083.5 (553), 1044.4 (2), 916.4 (196), 516.2 (111), 485.2(86),468.9 (105), 422.2 (116), 157.5 (4), 24.9 (3), 17.3 (1)
$O^{11}B(OH)$·OH (C_s, $^2A''$)	−251.790 705 (−251.242 535)	3699.9 (31), 3597.2 (913), 2073.5 (489), 1055.0(74), 1032.7 (125), 527.4 (39), 527.2 (13),411.5 (209), 318.5 (173), 181.1 (0), 76.0 (124), 65.2 (1)
TS (C_s, $^2A'$)	−251.786 365 (−251.235 944)	3856.5 (209), 3735.5 (36), 2029.1 (534), 1029.7 (3),942.1 (166), 518.0 (59), 492.4 (114), 426.6 (89), 214.9 (9), 155.9 (224), 87.1 (84), 117.1i (12)

[a] In hartree, after zero point energy corrections; the values in parentheses are single point energies calculated at the CCSD(T)/6-311++G(d,p) level.

TABLE 3: Comparisons between the Calculated and Experimentally Observed Vibrational Frequencies (cm^{-1}) and Isotopic Frequency Ratios of the $OB(OH)_2$ and OH·OB(OH) Complex

		freq		$^{11}B/^{10}B$ (^{16}O)		$^{16}O/^{18}O$ (^{10}B)	
molecule	mode	calcd	obsd	calcd	obsd	calcd	obsd
OH·$O^{11}B(OH)_2$	a′ (OH str)	3864.7	3686.0	1.0000	1.0000	1.0032	1.0031
(C_s, $^2A'$)	a′ (OH str)	3863.0	3673.5	1.0000	1.0000	1.0032	1.0031
	a′ (B−OH str)	1459.9	1405.2	1.0351	1.0601	1.0109	1.0156
	a′ (B−OH str)	1323.6	1339.7	1.0327	1.0237	1.0149	1.0383
	a′ (BOH bend)	994.7	999.6	1.0001	1.0017	1.0086	1.0096
	a′ (BOH bend)	978.8	984.8	1.0018	1.0015	1.0160	1.0111
	a″ (BO_3 def)	642.1	648.0	1.0396	1.0394	1.0094	
OH·$O^{11}B(OH)$	a′ (OH str)	3875.9	3665.3	1.0000	1.0000	1.0033	1.0032
(C_s, $^2A''$)	a′ (OH str)	3600.5	3447.5	1.0000	1.0000	1.0033	1.0032
	a′ (*B*═O str)	2083.4	2037.0	1.0353		1.0144	
	a′ (BOH bend)	916.2	892.5	1.0069	1.0071	1.0105	1.0124

The *cis*−*trans*-$OB(OH)_2$ molecule is photosensitive; it decomposed to form the metaboric acid and hydroxyl radical upon broad-band UV−visible irradiation. The in situ formed OB(OH) and OH fragments cannot escape the matrix cage and recombine to form the hydrogen-bonded OH·OB(OH) complex due to the matrix cage effect. Upon sample annealing, the OH·OB(OH) complex absorptions disappeared while the $OB(OH)_2$ absorptions increased. This implies that the OH·OB(OH) complex recombines to give *cis*−*trans*-$OB(OH)_2$. The observation of this process on annealing indicates that the recombination process requires very low activation energy.

Water adsorption and hydrolysis on molecular transition metal dioxides and oxyhydroxides has been investigated theoretically.[32] The $MO_2 + H_2O$ reactions were determined to proceed via the initial formation of a stable water complex as intermediate followed by one hydrogen atom transfer from water to one oxygen atom in MO_2. The reaction comprises the breaking of one M═O bond and the formation of two OH groups to give $OM(OH)_2$. This reaction mechanism was confirmed by matrix isolation infrared spectroscopic study on the TiO_2 and $SiO_2 + H_2O$ reaction.[33,34] The present experimental observations indicate that the $BO_2 + H_2O$ reaction does not follow such reaction mechanism. As can be seen in Figure 5, the O−H stretching vibrations of *cis*−*trans*-$OB(OH)_2$ shifted only when isotopic substituted $^{18}O_2 + H_2O$ sample was used. Both modes show no shift when the $H_2{}^{18}O + O_2$ sample was used. These experimental observations indicate that both O atoms in the OH groups come from BO_2, while the terminal O atom in *cis*−*trans*-$OB(OH)_2$ originates from water. The $BO_2 + H_2O$ reaction proceeds in a concerted process with both hydrogen atoms transfering to BO_2 in forming *cis*−*trans*-$OB(OH)_2$.

Theoretical calculations indicate that the *cis*−*trans*-$OB(OH)_2$ molecule decomposes to form the OB(OH) and OH fragments via a transition state (Figure 7, TS). This process is endothermic by 42.7 kcal/mol with a barrier height of 46.1 kcal/mol (CCSD(T)//B3LYP). Experimentally, the formation of the OH·OB(OH) complex is a photochemical process and most likely involves an electronically excited-state of $OB(OH)_2$. In the present experiments, broad-band UV−visible light from a high-pressure mercury arc lamp (250−580 nm) was employed for irradiation, but filtered experiments indicated that only the light in the wavelength range of 250−300 nm is responsible for dissociation. The photon energy in this wavelength range is sufficient to overcome the energy barrier for dissociation reaction from $OB(OH)_2$ to the OH·OB(OH) complex. According to theoretical calculations, the reversed OH·OB(OH) → *cis*−*trans*-$OB(OH)_2$ association reaction has a very low energy barrier of 3.4 kcal/mol. Therefore, the association reaction between

OB(OH) and HO radical is able to proceed spontaneously upon sample annealing.

Conclusions

The hydrolysis of molecular boron dioxide has been investigated using matrix isolation infrared absorption spectroscopy as well as theoretical calculations. The boron dioxide molecules were prepared by the reactions of laser-evaporated boron atoms with dioxygen. In solid argon, the boron dioxide molecules reacted with water molecules to give the $OB(OH)_2$ molecules spontaneously on annealing. The $OB(OH)_2$ molecule was characterized to have a doublet ground-state with two OH groups in the cis−trans form. The isotopic substitution experiments indicate that the hydrolysis process proceeds via a concerted two hydrogen atom transfer mechanism. The *cis*−*trans*-$OB(OH)_2$ molecule decomposes to form the OH·OB(OH) complex upon broad-band UV−visible irradiation. The OH·OB(OH) complex is predicted to have a $^2A''$ ground-state with a bent C_s symmetry, in which the terminal oxygen atom of the OB(OH) fragment is hydrogen bonded with the hydroxyl radical. The OH·OB(OH) complex recombines to the *cis*−*trans*-$OB(OH)_2$ molecule upon sample annealing.

Acknowledgment. Financial support from the National Basic Research Program of China (Grant No. 2007CB815203) and the National Natural Science Foundation of China (Grant No. 20433080) is gratefully acknowledged.

References and Notes

(1) Yetter, R. A.; Rabitz, H.; Dryer, F. L.; Brown, R. C.; Kolb, C. E. *Combust. Flame* **1991**, *83*, 43.

(2) (a) Attinà, M.; Cacace, F.; Grandinetti, F.; Occhiucci, G.; Ricci, A. *Int. J. Mass Spectrom. Ion Proc.* **1992**, *117*, 47. (b) Attinà, M.; Cacace, F.; Occhiucci, G.; Ricci, A. *Inorg. Chem.* **1992**, *31*, 3114. (c) Attinà, M.; Cacace, F.; Ricci, A.; Grandinetti, F.; Occhiucci, G. *J. Chem. Soc., Chem. Commun.* **1991**, 66.

(3) White, D.; Mann, D. E.; Walsh, P. N.; Sommer, A. *J. Chem. Phys.* **1960**, *32*, 488.

(4) Meschi, D. J.; Chupka, W. A.; Berkowitz, J. *J. Chem. Phys.* **1960**, *33*, 530.

(5) Randall, S. P.; Margrave, J. L. *J. Inorg. Nucl. Chem.* **1960**, *16*, 29.

(6) Gilson, T. R. *J. Chem. Soc., Dalton Trans.* **1991**, 2463.

(7) Ogden, J. S.; Young, N. A. *J. Chem. Soc., Dalton Trans.* **1988**, 1645.

(8) Andrews, L.; Burkholder, T. R. *J. Chem. Phys.* **1992**, *97*, 7203.

(9) (a) Wang, W.; Zhang, Y.; Huang, K. *J. Phys. Chem. B* **2005**, *109*, 8562. (b) Wang, W.; Zhang, Y.; Huang, K. *Chem. Phys. Lett.* **2005**, *405*, 425.

(10) Elango, M.; Parthasarathi, R.; Subramanian, V.; Sathyamurthy, N. *J. Phys. Chem. A* **2005**, *109*, 8587.

(11) Zapol, P.; Curtiss, L. A.; Erdemir, A. *J. Chem. Phys.* **2000**, *113*, 3338.

(12) Zaki, K.; Pouchan, C. *Chem. Phys. Lett.* **1995**, *236*, 184.

(13) Enyashin, A. N.; Ivanovskii, A. L. *Chem. Phys. Lett.* **2005**, *411*, 186.

(14) Duan, X.; Linder, D. P.; Page, M.; Soto, M. R. *J. Mol. Struct. (THEOCHEM)* **1999**, *465*, 231.

(15) Zaki, K.; Pouchan, C. *J. Chemie. Physique.* **1996**, *93*, 563.

(16) Ramondo, F.; Bencivenni, L.; Sadun, C. *J. Mol. Struct. (THEOCHEM)* **1990**, *68*, 101.

(17) Lapicki, A.; Peiris, D. M.; Smolanoff, J. N.; Anderson, S. L. *J. Phys. Chem. A* **1999**, *103*, 226.

(18) (a) Wang, G. J.; Zhou, M. F. *Int. Rev. Phys. Chem.* **2008**, *27*, 1. (b) Zhou, M. F.; Tsumori, N.; Xu, Q.; Kushto, G. P.; Andrews, L. *J. Am. Chem. Soc.* **2003**, *125*, 11371. (c) Wang, G. J.; Gong, Y.; Chen, M. H.; Zhou, M. F. *J. Am. Chem. Soc.* **2006**, *128*, 5974.

(19) Frisch, M. J.; Trucks, G. W.; Schlegel, H. B.; Scuseria, G. E.; Robb, M. A.; Cheeseman, J. R.; Montgomery, J. A., Jr.; Vreven, T.; Kudin, K. N.; Burant, J. C.; Millam, J. M.; Iyengar, S. S.; Tomasi, J.; Barone, V.; Mennucci, B.; Cossi, M.; Scalmani, G.; Rega, N.; Petersson, G. A.; Nakatsuji, H.; Hada, M.; Ehara, M.; Toyota, K.; Fukuda, R.; Hasegawa, J.; Ishida, M.; Nakajima, T.; Honda, Y.; Kitao, O.; Nakai, H.; Klene, M.; Li, X.; Knox, J. E.; Hratchian, H. P.; Cross, J. B.; Adamo, C.; Jaramillo, J.; Gomperts, R.; Stratmann, R. E.; Yazyev, O.; Austin, A. J.; Cammi, R.; Pomelli, C.; Ochterski, J. W.; Ayala, P. Y.; Morokuma, K.; Voth, G. A.; Salvador, P.; Dannenberg, J. J.; Zakrzewski, V. G.; Dapprich, S.; Daniels, A. D.; Strain, M. C.; Farkas, O.; Malick, D. K.; Rabuck, A. D.; Raghavachari, K.; Foresman, J. B.; Ortiz, J. V.; Cui, Q.; Baboul, A. G.; Clifford, S.; Cioslowski, J.; Stefanov, B. B.; Liu, G.; Liashenko, A.; Piskorz, P.; Komaromi, I.; Martin, R. L.; Fox, D. J.; Keith, T.; Al-Laham, M. A.; Peng, C. Y.; Nanayakkara, A.; Challacombe, M.; Gill, P. M. W.; Johnson, B.; Chen, W.; Wong, M. W.; Gonzalez, C.; Pople, J. A. *Gaussian 03, Revision B.05*; Gaussian, Inc.: Pittsburgh, PA, 2003.

(20) Becke, A. D. *J. Chem. Phys.* **1993**, *98*, 5648.

(21) Lee, C.; Yang, W.; Parr, R. G. *Phys. Rev. B* **1988**, *37*, 785.

(22) (a) McLean, A. D.; Chandler, G. S. *J. Chem. Phys.* **1980**, *72*, 5639. (b) Krishnan, R.; Binkley, J. S.; Seeger, R.; Pople, J. A. *J. Chem. Phys.* **1980**, *72*, 650.

(23) Burkholder, T. R.; Andrews, L. *J. Chem. Phys.* **1991**, *95*, 8697.

(24) Chertihin, G. V.; Andrews, L. *J. Chem. Phys.* **1998**, *108*, 6404.

(25) Andrews, L.; Burkholder, T. R. *J. Phys. Chem.* **1991**, *95*, 8554.

(26) Gajhede, M.; Larsen, S.; Rettrup, S. *Acta Crystallogr., Sect. B* **1986**, *42*, 545.

(27) Freyhardt, C. C.; Wiebcke, M. *J. Chem. Soc., Chem. Commun.* **1994**, 1675.

(28) Cheng, B. M.; Lee, Y. P.; Ogilvie, J. F. *Chem. Phys. Lett.* **1988**, *151*, 109.

(29) (a) Cooper, P. D.; Kjaergaard, H. G.; Langford, V. S.; McKinley, A. J.; Quickenden, T. I.; Schofield, D. P. *J. Am. Chem. Soc.* **2003**, *125*, 6048. (b) Langford, V. S.; McKinley, A. J.; Quickenden, T. I. *J. Am. Chem. Soc.* **2000**, *122*, 12859.

(30) Xie, Y. M.; Schaefer, H. F., III *J. Chem. Phys.* **1993**, *98*, 8829.

(31) Wang, B.; Hou, H.; Gu, Y. *Chem. Phys. Lett.* **1999**, *303*, 96.

(32) (a) Johnson, J. R. T.; Panas, I. *Inorg. Chem.* **2000**, *39*, 3181. (b) Johnson, J. R. T.; Panas, I. *Inorg. Chem.* **2000**, *39*, 3192.

(33) Shao, L. M.; Zhang, L. N.; Chen, M. H.; Lu, H.; Zhou, M. F. *Chem. Phys. Lett.* **2001**, *343*, 178.

(34) Zhou, M.; Zhang, L.; Lu, H.; Shao, L.; Chen, M, *J. Mol. Struct.* **2002**, *605*, 249.

JP8014172